Systemic Delivery of an Oncolytic Adenovirus Expressing Decorin for the Treatment of Breast Cancer Bone Metastases

Yuefeng Yang,[1,†] Weidong Xu,[1,†] Thomas Neill,[2] Zebin Hu,[3] Chi-Hsiung Wang,[4] Xianghui Xiao,[5] Stuart R. Stock,[6] Theresa Guise,[7] Chae-Ok Yun,[8] Charles B. Brendler,[4] Renato V. Iozzo,[2] and Prem Seth[1,*]

[1]*Gene Therapy Program, Department of Medicine, NorthShore Research Institute, An Affiliate of the University of Chicago, Evanston, Illinois;* [2]*Department of Pathology, Anatomy and Cell Biology and the Cancer Cell Biology and Signaling Program, Kimmel Cancer Center, Thomas Jefferson University, Philadelphia, Pennsylvania;* [3]*1st Division of In Vitro Diagnostic Reagents, National Institutes for Food and Drug Control, Beijing, China;* [4]*Department of Surgery, NorthShore Research Institute, Evanston, Illinois;* [5]*Advanced Photon Source, Argonne National Lab., Argonne, Illinois;* [6]*Department of Cell and Molecular Biology, Northwestern University, Chicago, Illinois;* [7]*Department of Medicine, Indiana University, Indianapolis, Indiana;* [8]*Department of Bioengineering, Hanyang University, Seoul, Korea.*
[†]*These two authors contributed equally to this work.*

The development of novel therapies for breast cancer bone metastasis is a major unmet medical need. Toward that end, we have constructed an oncolytic adenovirus, Ad.dcn, and a nonreplicating adenovirus, Ad(E1-).dcn, both containing the human decorin gene. Our *in vitro* studies showed that Ad.dcn produced high levels of viral replication and the decorin protein in the breast tumor cells. Ad(E1-).dcn-mediated decorin expression in MDA-MB-231 cells downregulated the expression of Met, β-catenin, and vascular endothelial growth factor A, all of which are recognized decorin targets and play pivotal roles in the progression of breast tumor growth and metastasis. Adenoviral-mediated decorin expression inhibited cell migration and induced mitochondrial autophagy in MDA-MB-231 cells. Mice bearing MDA-MB-231-luc skeletal metastases were systemically administered with the viral vectors, and skeletal tumor growth was monitored over time. The results of bioluminescence imaging and X-ray radiography indicated that Ad.dcn and Ad(E1-).dcn significantly inhibited the progression of bone metastases. At the terminal time point, histomorphometric analysis, micro-computed tomography, and bone destruction biomarkers showed that Ad.dcn and Ad(E1-).dcn reduced tumor burden and inhibited bone destruction. A nonreplicating adenovirus Ad(E1-).luc expressing the luciferase 2 gene had no significant effect on inhibiting bone metastases, and in several assays, Ad.dcn and Ad(E1-).dcn were better than Ad.luc, a replicating virus expressing the luciferase 2 gene. Our data suggest that adenoviral replication coupled with decorin expression could produce effective antitumor responses in a MDA-MB-231 bone metastasis model of breast cancer. Thus, Ad.dcn could potentially be developed as a candidate gene therapy vector for treating breast cancer bone metastases.

INTRODUCTION

BREAST CANCER IS THE SECOND LEADING CAUSE of cancer-related deaths among women in the United States. During the advanced stages of breast cancer, a majority of patients will eventually develop bone metastases.[1–4] Bone metastases cause osteolytic bone destruction, accompanied with bone pain, pathologic fractures, spinal cord compression, and hypercalcemia, resulting in morbidity and eventually mortality.[5,6] Bisphosphonates (BPs), and denosumab, an antibody against the receptor activator of nuclear factor kappa-B ligand (RANKL), are the two major available drugs for the treatment of bone metastases.[7,8] Both modalities primarily target tumor-induced bone resorption/loss, and can reduce skeletal related events. However, they are not effective in destroying the established bone metastases and do not improve patients' survival.[9] Therefore, the development of novel therapies to treat bone metastases of breast cancer is an unmet need in medicine.

The oncolytic adenoviruses, which can selectively replicate and kill the tumor cells, represent a promising gene therapy approach for the treatment

*Correspondence: Dr. Prem Seth, Gene Therapy Program, Department of Medicine, NorthShore Research Institute, An Affiliate of the University of Chicago, Evanston Hospital, 2650 Ridge Avenue, Room B 652, Evanston, IL 60201. E-mail: pseth@northshore.org

DOI: 10.1089/hum.2015.098

of cancer. During the progression of bone metastasis, many growth factors and cytokines are released into the bone microenvironment and interact with tumor cells to promote skeletal tumor growth and bone destruction.[10,11] Our laboratory is interested in developing oncolytic adenoviruses targeting the microenvironment of bone metastases in breast and prostate cancers.[12–18] Here, we have examined if an oncolytic adenovirus expressing decorin can be developed for treating breast cancer bone metastases. Decorin, a member of the small leucine-rich proteoglycan gene family,[19] has been identified as an inhibitor of transforming growth factor-β (TGF-β) signaling, known to play a pivotal role in bone metastases.[20,21] Decorin can also regulate tumor cell proliferation, invasion, and migration and inhibit tumor angiogenesis.[22–25] Moreover, decorin reprograms the tumor microenvironment, evokes endothelial cell autophagy via AMPKα,[19,26] and triggers tumor cell mitophagy in a mitostatin-dependent manner.[27,28] In breast cancer patients, low levels of decorin in the tumor microenvironment are associated with a more aggressive disease phenotype.[29,30] Decorin has also been identified as being substantially downregulated in an unbiased RNA-seq screen for hepatocellular carcinoma.[31] The adenoviral-mediated delivery of decorin has been shown to inhibit tumorigenic growth in orthotopic xenograft models.[32–34] However, the therapeutic effect of an adenovirus expressing decorin on breast cancer bone metastases has not been previously investigated. Therefore, the purpose of this study is to examine if overexpressing decorin via an oncolytic adenovirus could be potentially developed for the treatment of breast cancer bone metastases. We first examined if Ad.dcn can replicate in breast tumor cells and produce decorin protein. Next, we examined if decorin expression in breast tumor cells was functionally active and could inhibit selected tyrosine kinase growth factor receptors, pro-angiogenic molecules, block cell migration, and induce mitochondrial autophagy (mitophagy). Finally, we investigated if systemic delivery of Ad.dcn could inhibit bone metastases and tumor-induced bone destruction in MDA-MB-231 breast cancer model in nude mice. Based on our *in vitro* and *in vivo* studies described here, we believe that Ad.dcn is promising for targeting bone metastases of breast cancer.

MATERIALS AND METHODS

Cell lines and adenoviruses

The human breast tumor cell line MCF-7 was purchased from ATCC and cultured in EMEM medium containing 10% fetal calf serum (FCS). Human breast tumor cell line MDA-MB-231 was kindly provided by Dr. Theresa Guise, and cultured in DMEM containing 10% FCS. MDA-MB-231-luc cell line was generated by stably transfecting with a retrovirus expressing the luciferase2 (*luc2*) gene into parental MDA-MB-231 cells as described.[13] All the medium components were purchased from Invitrogen. Ad.dcn and Ad.luc, oncolytic adenoviruses expressing decorin and *luc2* genes, respectively, were constructed using *dl*01/07 (an adenoviral mutant harboring two mutations in the *E1A* gene) genomic DNA as described.[18] Nonreplicating adenoviruses Ad(E1-).dcn, Ad(E1-).luc, and Ad(E1-).null were generated using the Ad-easy system.[13,16,18] All the adenoviruses were grown in 293 cells and purified by CsCl density gradients as previously described.[16,18]

Adenoviral replication assay

MDA-MB-231 and MCF-7 cells were seeded into 6-well plates at a density of 3×10^5 cells per well. Next day, the cells were infected with adenoviruses (2.5×10^4 VPs/cell) for 3 hr. After washing the cells three times with the medium, crude cell lysates were collected immediately or at 48 hr after viral infections. The cell lysates were used to infect HEK 293 cells for 48 hr and the cells were stained for hexon expression using Adeno-X Rapid titer kit (Clontech) as described previously.[15] Hexon-expressing positive brown cells were photographed under a microscope, and at least five different fields were counted to quantify the viral replication. Viral burst size, an increase of hexon-expressing positive cells from 3 to 48 hr, was used as an indicator of viral replication.

Adenoviral cytotoxicity assay

MDA-MB-231 and MCF-7 cells were seeded into 96-well plates (1×10^3 cells/well). The next day, cells were infected with various doses of adenoviruses (ranging from 32 viral particles per cell (VPs/cell) to 1.25×10^6 VPs/cell). Incubations were continued for 7 days. Cell survival was determined by the sulforhodamine B staining assay as previously described.[35]

Decorin expression in the breast tumor cells

MDA-MB-231 and MCF-7 cells were plated into each well of a 6-well plate (3×10^5 cells per well). The following day, cells were infected with various adenoviruses (2.5×10^4 VPs/cell). After 24 hr, the medium was replaced by a fresh serum-free medium, and the incubations continued for another 24 hr. Cell lysates and medium were collected. The decorin protein in the cells and the medium were

examined by Western blotting using a mouse antihuman decorin antibody according to the published methods.[18] The decorin protein in the medium was also examined by enzyme-linked immunosorbent assay (ELISA) using mouse antihuman decorin antibody and botinylated mouse antihuman decorin antibody (R&D Systems) using previously described methods.[18]

Gene expression analysis of decorin target genes

MDA-MB-231 cells were infected with Ad(E1-).dcn or Ad(E1-).null (2.5×10^4 VPs/cell). Forty-eight hours postinfection, total RNA was isolated from the cells and subjected to a DNaseI digestion to eliminate potentially contaminating genomic DNA and viral plasmids, followed by cDNA synthesis. Quantitative polymerase chain reaction (Q-PCR) was conducted to detect the expression of decorin and decorin-regulated genes (*MET*, *CTNNB1*, and *VEGFA*). Gene expression was normalized to *ACTB*, an endogenous housekeeping gene, by using comparative ΔΔCT methods. The protein abundance of Met, β-catenin, and VEGFA was also analyzed at 48 hr after infection with Ad(E1-).dcn or Ad(E1-).null (2.5×10^4 VPs/cell or 5×10^4 VPs/cell) by Western blotting and normalized to GAPDH, as previously described.[18,23,36]

Cell migration assays

MDA-MB-231 cells were infected with Ad.dcn or Ad.luc for 6 hr. Cells were washed three times and were cultured in serum-free medium for another 24 hr. The medium was collected and subjected to ultracentrifugation to remove cell debris and any adenoviral particles. The concentration of decorin in this conditioned medium was determined to be about 3 μg/ml. For transwell migration assay, MDA-MB-231 cells (5×10^4) were plated into the upper chamber with the conditioned medium. Conditioned medium was also added to the lower chamber. After 24 hr, the cells that migrated to the lower surface of the filter were fixed, and stained using the manufacturer's protocol (Fisher Scientific). The cells were counted in 5 randomly selected views using 100× magnifications. For the scratch wound-healing assay, confluent MDA-MBA-231 cells were scratched to generate wounds as described,[18] and then incubated with the conditioned medium for 0, 16, or 24 hr. Live cell images were taken (Nikon DS-Fi1 camera). The distances between the two margins of the wounds were measured using the Nikon image software, and percentages of wound area filled were determined and analyzed as described previously.[18]

Mitochondrial autophagy analysis

MDA-MB-231 cells were infected with Ad(E1-).null or Ad(E1-).dcn (2.5×10^4 VPs/cell). Forty-eight hours postinfection, DNA samples containing both mitochondrial DNA (mtRNA) and nuclear genomic DNA were prepared as reported previously.[28] NADH dehydrogenase I (*ND1*), as a mtDNA marker, and nuclear genomic DNA-encoded lipoprotein lipase (*LPL*) were determined by Q-PCR. The relative mtDNA contents were calculated by comparative ΔΔCT methods, using *LPL* as a control gene.

To detect mitophagy-related morphological changes, MDA-MB-231 cells were stably transfected with Su9-GFP, a mitochondrial fusion protein, and then infected with Ad(E1-).null or Ad(E1-).dcn (2.5×10^4 VPs/cell). After a 24 hr incubation period, cells were imaged by fluorescence microscopy. All fluorescence images were taken with the same exposure, gain, and intensity. Mitochondrial morphological parameters, including mitochondrial number, area, length, and form factors, were quantified using a legacy version of ImageJ (v1.38) as published previously.[37]

Breast cancer bone metastases model, bioluminescence imaging, and X-ray radiography

All the animal experimental procedures were approved by the Institute of Animal Care and Use Committee at NorthShore University HealthSystem. MDA-MB-231-luc cells were injected into the left heart ventricle (day 0) (1.0×10^5 cells/mouse) of 5-week-old female mice (Nu/Nu) (Charles River Laboratories). On day 9, mice were subjected to bioluminescence imaging (BLI) using Xenogen IVIS spectrum imaging equipment as previously described.[13,15] Red circles were drawn around the regions of interest (ROIs) in the hind limbs. Signal intensity was quantified as the total flux (photons/sec) within the ROIs as positioned over the left and right hind limbs using Living Image software 3.0 (Caliper Life Sciences). Mice with bone metastases in the hind limbs were divided into 5 groups (10 mice per group), each group with nearly equal photon signals in the hind limbs. On days 10, 12, and 15, adenoviruses were administrated via tail vein (each injection 2.5×10^{10} VPs/mouse). Bone metastases were also examined on days 10, 16, and 22 after cell injection by radiography using an LX-60 system with a digital camera (Faxitron X-Ray) using published methods.[13] On day 22 (terminal time point), bone metastases were also examined by BLI. Only the photon signals in the ROIs in the hind limbs were used to quantify the skeletal metastases.

Bone histology and histomorphometry

Mice were euthanized on day 22 after cell injection, and hind limbs were collected and processed. The tissue sections were stained with hematoxylin and eosin (H&E), and tumor burden in the tibia/femur was quantified as described earlier.[13,15] Tissue sections were subjected to tartrate-resistant acid phosphatase (TRAP) staining, and multinucleated TRAP-positive osteoclasts were counted at the bone–tumor interface according to the methods previously described.[13]

Synchrotron micro-computed tomography

Synchrotron micro-computed tomography (microCT), which can provide high spatial resolution and contrast sensitivity of the imaged volumes of the bones, was conducted. Data from the representative proximal tibiae of each treatment group were collected at beamline 2-BM of the Advanced Photon Source at Argonne National Laboratory (Argonne, IL) using the microCT instrument. The following conditions were used for data collection: 15 keV, 0.12° rotation increment, 180° rotation range. The reconstructed slices were 2K × 2K in size and consisted of 2.96 μm isotropic volume elements (voxels). From within the constructed volume, 3D images of bone sections spanning about 3.0 mm below the growth plate regions were produced using Amira 5.3.2 software (Visage Imaging).

Measurement of serum calcium levels

At the terminal time point, the blood was collected by cardiac puncture, and centrifuged for 10 min at 10,000 rpm to obtain the sera. Calcium levels in the serum were measured using the QuantiChrom calcium assay kit (BioAssay System) as described earlier.[12]

Statistical analysis

Data are presented as mean ± standard error of the mean (SEM). Statistical analyses were conducted using GraphPad Prism software version 5 (GraphPad Software). Longitudinal data were analyzed by using a two-way repeated measure ANOVA followed by Bonferroni *post hoc* pair wise tests for all data of the time course. Student's *t*-tests were conducted to compare the expression of various decorin targets, mtDNA content, and mitochondrial autophagy parameters between Ad(E1-).null and Ad(E1-).dcn-infected cells. To analyze the data involving three or more treatment groups, one-way ANOVA followed by Bonferroni *post hoc* tests were performed. Differences were considered significant at two-sided $p < 0.05$.

RESULTS

Ad.dcn replication, viral-induced cytotoxicity, and decorin production in the breast tumor cell lines

Ad.dcn, a recombinant adenovirus carrying the human decorin gene, was constructed using *dl*01/07 backbone containing two mutations in the *E1A* gene (Fig. 1A) as previously described.[18] Ad(E1-).dcn, a nonreplicating adenovirus also carrying the human decorin gene, was constructed using the Ad-easy system as described.[18] Ad.luc, an oncolytic adenovirus expressing the *luc2* gene, and Ad(E1-).luc, a nonreplicating adenovirus containing the *luc2* gene, were constructed as previously described.[15,16] The replication potential of Ad.dcn, Ad(E1-).dcn, Ad.luc, and Ad(E1-).luc was examined in two human breast tumor cell lines, MDA-MB-231 and MCF-7. There was an increase in viral titers by about 500-fold when cells were infected with Ad.dcn or Ad.luc; however, there was no increase in the viral titers after infection with Ad(E1-).dcn or Ad(E1-).luc (Fig. 1B). Moreover, Ad.dcn and Ad.luc produced a dose-dependent cytotoxicity in MDA-MB-231 and MCF-7 cells. Based on the IC_{50} values (viral dose required to kill 50% of the cells), Ad.dcn and Ad.luc were about 50 times more cytotoxic than Ad(E1-).dcn and Ad(E1-).luc (Fig. 1C and D). Western blot analysis of the breast tumor cell lysates and the medium confirmed decorin expression after infection with Ad.dcn and Ad(E1-).dcn (Fig. 1E). The analysis of decorin protein expression in the extracellular medium by the ELISA indicated that Ad.dcn infection produced higher amounts of decorin compared to Ad(E1-).dcn-infected cells (Fig. 1F). These results suggest that infection of the breast tumor cells with Ad.dcn results in viral replication and cytotoxicity. Moreover, the infection of tumor cells with Ad.dcn or Ad(E1-).dcn produces the decorin protein, which is also released into the extracellular medium.

Adenoviral-mediated decorin production reduces Met, β-catenin, and vascular endothelial growth factor A expression, and inhibits the migration of MDA-MB-231 cells

The infection of MDA-MB-231 cells with Ad(E1-).dcn produced *DCN* mRNA, and resulted in the downregulation of *MET* (c-Met), *CTNNB1* (β-catenin), and *VEGFA* (vascular endothelial growth factor A) transcripts (Fig. 2A). Consistent with the mRNA changes, significant reductions in Met, β-catenin, and VEGFA proteins were also observed (Fig. 2B and C). We also attempted to examine if

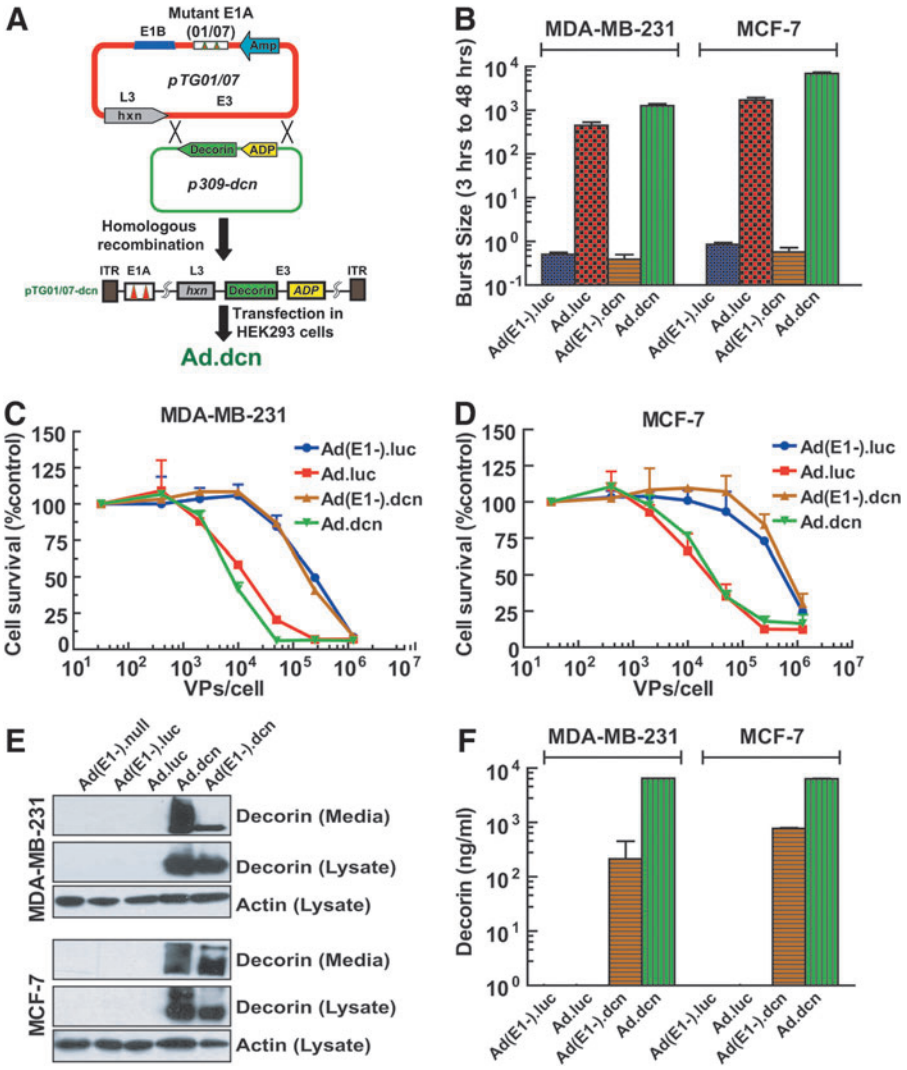

Figure 1. Construction of oncolytic adenovirus Ad.dcn, and analyses of viral replication, viral-induced cytotoxicity, and protein expression in human breast tumor cells. **(A)** Construction of Ad.dcn. The human decorin gene was cloned into the shuttle plasmid, p309, and then subjected to homologous recombination with an adenovirus backbone plasmid pTG01/07, which has two deletions in E1A region. **(B)** Adenovirus replication in breast tumor cells. MDA-MB-231 and MCF-7 cells were infected with 2.5×10^4 VPs/cell of Ad(E1-).dcn, Ad.dcn, Ad(E1-).luc, or Ad.luc. After a 3 hr incubation, cells were washed three times with the medium, and then crude cellular lysates were collected immediately or 48 hr after the initial viral infection. The viral burst sizes were examined in HEK293 cells, and the ratios of burst sizes of 48 and 3 hr were calculated. **(C, D)** Adenoviral-induced cytotoxicity in breast tumor cells. MDA-MB-231 and MCF-7 cells were infected with various adenoviruses using serial viral dilutions, ranging from 32 to 1.25×10^6 VPs/cell. After 7 days of incubation, cell survival was analyzed by sulforhodamine B (SRB) staining. In this cell survival method using SRB staining, the cells are plated in 96-well plates, and the outer most wells are used as control wells. Unfortunately, in the 96-well plates, cells in the outer wells tend to grow a bit slower, perhaps because of an uneven CO_2/moisture gradient across various wells. This notwithstanding, survival of the control cells is set at 100%; however, in some of the inner wells (treated with adenoviruses), there appear to be a slight increase in cell survival. This can result in a false increase of survival greater than 100%, as shown in panels C and D. **(E, F)** Decorin protein expression in the breast tumor cells. MDA-MB-231 and MCF-7 cells were infected by 2.5×10^4 VPs/cell of various adenoviruses in complete culture medium. After 24 hr, the medium was replaced by a fresh serum-free medium. After a 24 hr incubation, cell lysates and medium were collected. Decorin expression was analyzed by Western blotting (both cell lysates and medium) and ELISA (medium). Note that decorin is a proteoglycan, and can be detected either as the core protein or with the covalently attached glycosaminoglycan chain. Therefore, decorin protein bands appear as a polydispersant, as seen in the medium obtained from the Ad.dcn-infected cells. The data presented in panels B, C, D, and F are mean ± SEM of three independent experiments. Data in panel E are a typical Western blot showing decorin expression. ELISA, enzyme-linked immunosorbent assay.

there was any further inhibition of the target proteins by a higher dose (5×10^4 VPs/cell) of Ad(E1-).dcn. However, there was no further improvement in the inhibitory effects of Ad(E1-).dcn, indicating that the decorin protein had reached its maximal inhibitory effects at the lower viral dose (2.5×10^4 VPs/cell). In the experiments evaluating the function of vector-mediated decorin protein production *in vitro* (Fig. 2A–C), we chose to employ the nonreplicating adenoviral vectors, as the oncolytic viruses (Ad.luc and Ad.dcn) would potentially kill the cancer cells, thereby confounding

the results of our gene/protein expression and mitophagy analyses.

Next, we analyzed the effect of the decorin protein on the migration of MDA-MB-231 cells. Tumor cells were exposed to the conditioned medium containing decorin. Results obtained in the transwell migration showed that Ad.dcn-mediated decorin expression significantly inhibited migration of MDA-MB-231 cells (Fig. 2D). In the wound healing assay, the incubation of MDA-MB-231 cells with the decorin-containing conditioned medium for 16 or 24 hr resulted in a significant inhibition of cell migration across the scratched areas (Fig. 2E and F).

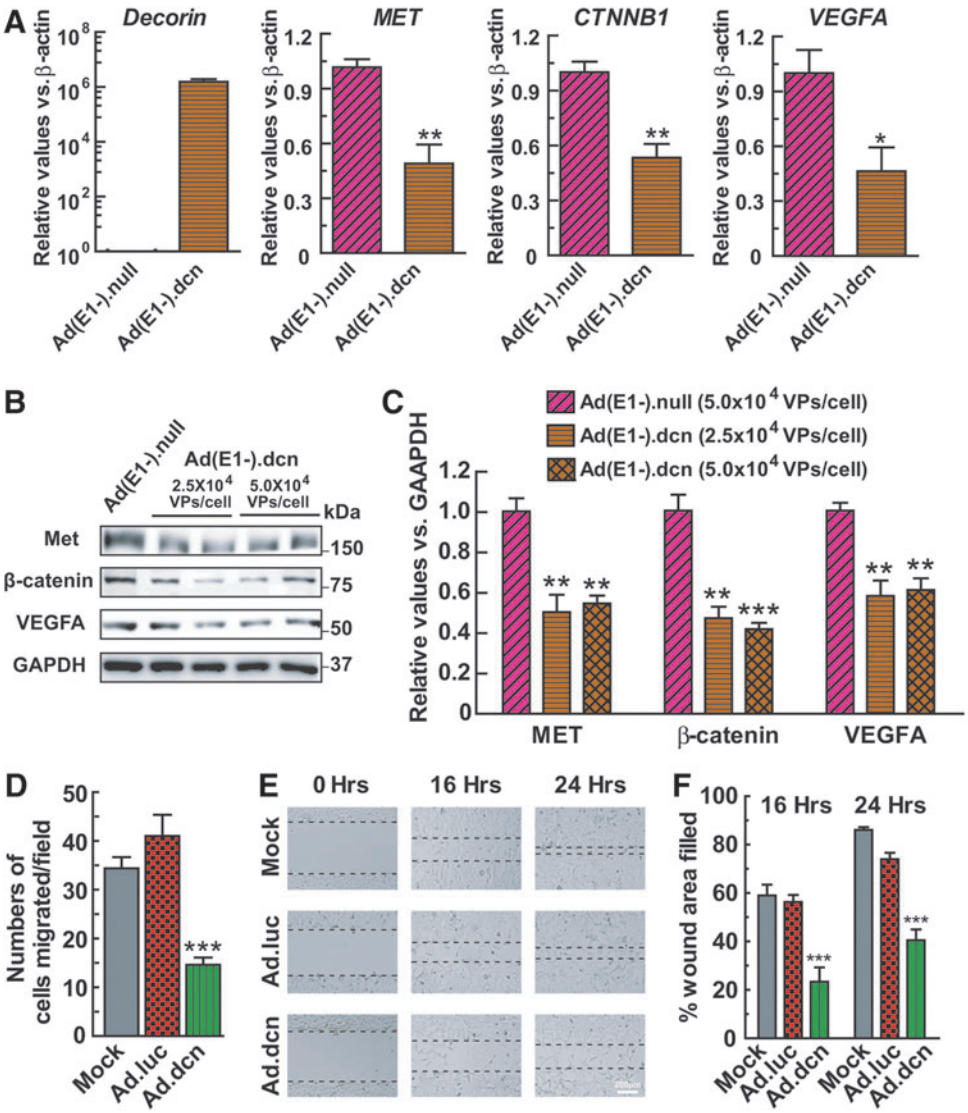

Figure 2. Adenoviral-mediated decorin expression decreased the expression of target genes, and reduced the migration of MDA-MB-231 cells *in vitro*. MDA-MB-231 cells were infected with 2.5×10^4 VPs/cell of Ad(E1-).null or Ad(E1-).dcn. Total RNA was isolated and cDNA was synthesized at 48 hr postinfection. All samples were subjected to a DNase I digestion that eliminates potentially contaminating genomic DNA and viral plasmids before cDNA synthesis. Then, Q-PCR was conducted to detect the expression of decorin and its target genes *MET*, *CTNNB1*, and *VEGFA* **(A)**. The protein expression of Met, β-catenin, and VEGFA was also detected by Western blotting at 48 hr after infection with Ad(E1-).null (5×10^4 VPs/cell) and Ad(E1-).dcn (2.5×10^4 VPs/cell or 5×10^4 VPs/cell) **(B)**. Quantitative analysis of protein expression is shown in **(C)**. **(D)** To analyze the effect of decorin on cell migration, the conditioned medium containing the decorin protein was prepared from the culture medium of mock, Ad.luc, or Ad.dcn (2.5×10^4 VPs/cell)-infected MDA-MB-231 cells. After incubation with the conditioned medium for 24 hr, the migration of MDA-MB-231 cells was examined by the transwell assay and is shown. **(E)** After incubation with the conditioned medium for 16 or 24 hr, the migration of MDA-MB-231 cells was also examined by the wound healing assay. The images were acquired using Nikon DS-Fi1 camera and the representative images are shown. The dotted lines define the gap distances between the two margins of the wounds that are measured using Nikon image software. Scale bar is 200 μm. **(F)** The wound healing area filled in for each experimental condition was measured using Nikon image software and is shown. The data presented in panels A, C, and D are mean $\pm$ SEM of three independent experiments. The data presented in panel F are mean $\pm$ SEM of four independent experiments (*$p<0.05$; **$p<0.01$; ***$p<0.001$). Panel B shows a typical Western blot of the various decorin targets.

Adenoviral-mediated expression of the decorin protein induces mitochondrial autophagy in the breast tumor cells

Next, we investigated if the adenoviral vector-mediated decorin production can induce mitochondrial autophagy in MDA-MB-231 cells. Compared with Ad(E1-).null, Ad(E1-).dcn infection significantly downregulated mitochondrial DNA (mtDNA) in MDA-MB-231 cells (Fig. 3A). Further, Ad(E1-).dcn evoked visible morphological changes by disrupting the tubular organization of the mitochondrial network in favor of a more compact, collapsed structure in the tumor cells; the white arrowheads in the Ad(E1-).dcn-treated cells indicate aggregated areas of the mitochondrial network (Fig. 3B). Several mitochondrial parameters were analyzed to quantify changes in mitochondrial morphology in MDA-MB-231 cells. Our data indicated that Ad(E1-).dcn infection increased the total mitochondrial number (Fig. 3C), while it significantly decreased the mitochondrial surface area and length (Fig. 3C). Mitochondrial form factor, a valid prognosticator for mitochondrial autophagy, was also evaluated. Compared with Ad(E1-).null-infected cells, the mitochondrial form factor was significantly reduced in Ad(E1-).dcn-infected cells (Fig. 3C), indicating an increased circular mitochondrial appearance typically associated with mitochondrial autophagy. These studies suggest that mitochondrial autophagy is induced by Ad(E1-).dcn in MDA-MB-231 cells.

Systemic delivery of Ad.dcn inhibited the progression of breast cancer bone metastases in nude mice

To examine the effect of adenoviral vectors in inhibiting bone metastases, MDA-MB-231-luc cells

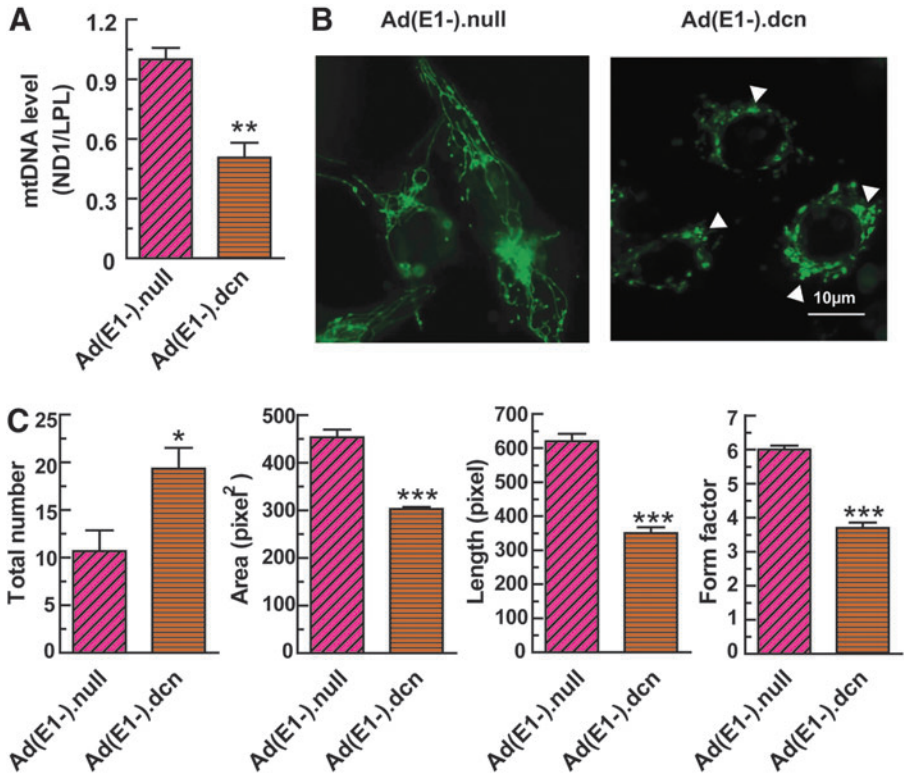

Figure 3. MDA-MB-231 cells undergo mitophagy after Ad(E1-).dcn infection. **(A)** Mitochondrial DNA (mtDNA) analysis. MDA-MB-231 cells were infected with 2.5×10^4 VPs/cell of Ad(E1-).dcn or Ad(E1-).null. Forty-eight hours later, total DNA was isolated and relative quantification of mtDNA was analyzed by Q-PCR. NADH dehydrogenase I (*ND1*) was used as a marker of mtDNA, and the expression of ND1 was normalized by nuclear genomic DNA-encoded lipoprotein lipase (*LPL*). **(B)** Mitochondrial morphology analysis. A plasmid encoding the mitochondrial fusion protein, Su9-GFP, was stably transfected into MDA-MB-231 cells and subsequently challenged with either 2.5×10^4 Ad(E1-).dcn or Ad(E1-).null. After a 24 hr incubation period, the Su9-GFP signal was imaged via fluorescence microscopy. Mitochondria are delineated as green. All fluorescence images were taken with the same exposure, gain, and intensity. White arrowheads indicate significant morphological changes of the mitochondrial network. Scale bar = 10 μm. **(C)** Quantification of mitochondrial morphological parameters using a legacy version of ImageJ (v1.38) encoded with a macro enabling quantification of various mitochondrial values for including total mitochondrial number, area, length, and form factor in the presence of Ad(E1-).null or Ad(E1-).dcn.[37] Data presented herein represent analyses that used at least $n=60$ MDA-MB-231 Su9GFP cells, with SEM plotted for each parameter. The data presented in panels A and C are mean ± SEM of three independent experiments (*$p<0.05$; **$p<0.01$; ***$p<0.001$).

were injected into the left cardiac ventricle (day 0) of female nude mice to establish bone metastases. On day 9, mice were screened via BLI for the presence of bone metastases. Mice bearing skeletal metastases were intravenously administered with buffer, Ad(E1-).dcn, Ad(E1-).luc, Ad.dcn, or Ad.luc adenoviral vectors using the dose and schedule described in Material and Methods. On day 22, whole-body bioluminescence images in the dorsal and ventral positions were taken. The BLI in the Ad(E1-).luc- and Ad.luc-treated groups could not be assessed as the large uptake of the luciferase-expressing viruses in the liver produces a strong BLI signal that subsequently masks the BLI signals from the MDA-MB-231-luc cells. The representative images of the other three groups are shown in Fig. 4A. Quantification of the combined signal intensity of dorsal and ventral hind limbs within the regions of interest (indicated by the red circles) was analyzed. The results indicated that the progression of bone metastases was inhibited significantly by Ad.dcn and Ad(E1-).dcn ($p < 0.001$ Ad.dcn vs. buffer group; $p < 0.01$ Ad(E1-).dcn vs. buffer group) (Fig. 4B).

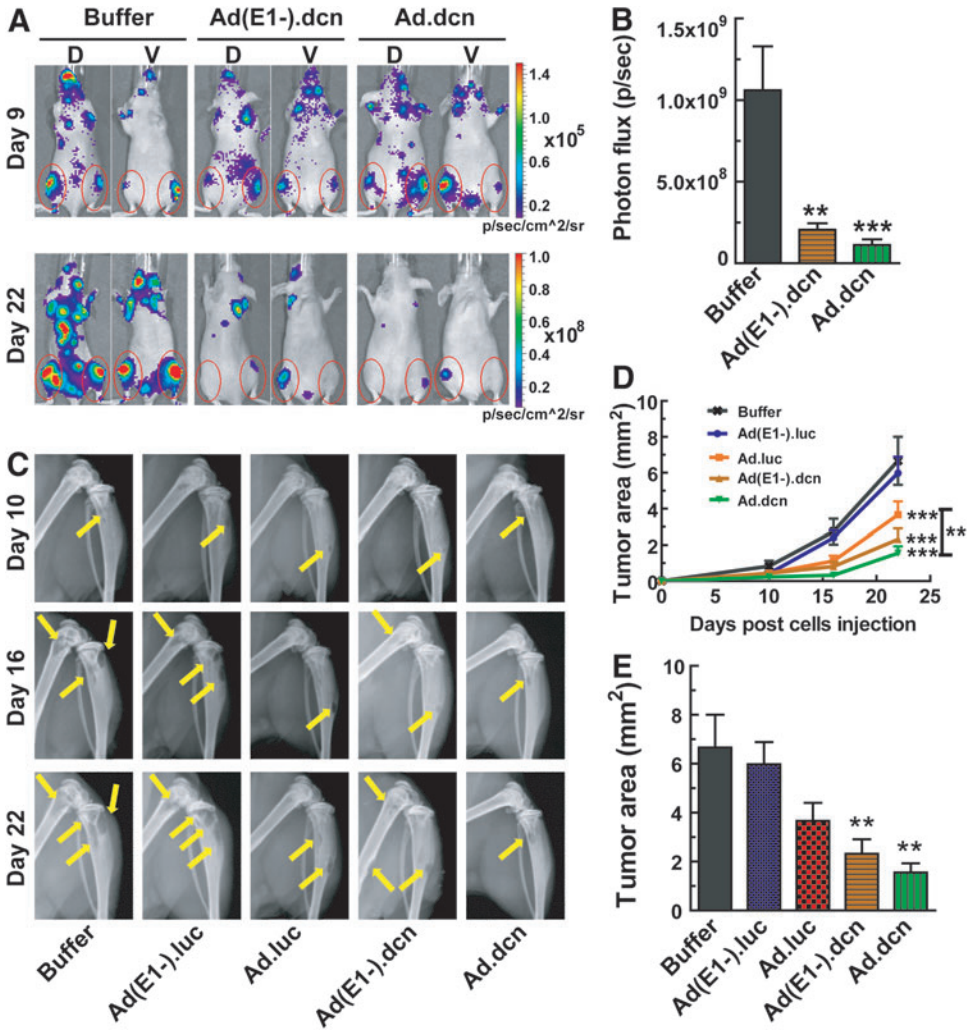

Figure 4. Effects of adenoviral vectors on progression of breast cancer bone metastases by BLI analysis and by radiographic analysis *in vivo*. MDA-MB-231-luc cells (1.0×10^5) were injected into the left heart ventricle (day 0) of 5-week-old female mice (Nu/Nu). On day 9, mice were subjected to BLI by using Xenogen IVIS spectrum imaging equipment. The photon signals in the hind limbs (within the regions of interest [ROIs] indicated by the red circles) were quantified. Mice with bone metastases in the hind limbs were divided into 5 groups (10 mice per group). On day 10, Ad(E1-).luc, Ad(E1-).dcn, Ad.luc, Ad.luc (2.5×10^{10} VPs/mouse), or buffer was systemically delivered via tail vein. Additional viral injections were also administered on days 12 and 15 (2.5×10^{10} VPs/injection/mouse). Representative whole-body BLI images on days 9 and 22 of the buffer, Ad(E1-).dcn, and Ad.dcn treatment groups are shown in **(A)**. The quantification of BLI signal intensities of combined dorsal and ventral hind limbs (within the ROIs) on day 22 is analyzed and is shown in **(B)**. Representative radiographs of mouse hind limbs on days 10, 16, and 22 are presented in the **(C)**, and the yellow arrows indicate the sites of osteolytic lesions. The progression of bone metastasis was monitored by quantification of lesion sizes in both hind limb bones and shown in **(D)**. The tumor area, indicated by lesion sizes, was calculated on day 22 and is shown in **(E)**. Data in panels B, D, and E were derived from 10 mice per group (*$p < 0.05$; **$p < 0.01$; ***$p < 0.001$).

To further evaluate bone metastases, radiographic measurements were conducted on days 10, 16, and 22. The representative images at each time point are shown in Fig. 4C, where the osteolytic lesions are indicated by the yellow arrows. The lesion sizes were calculated in the hind limbs of each mouse. The data indicated that Ad.dcn, Ad(E1-).dcn, and Ad.luc significantly inhibited the progression of bone metastases ($p < 0.001$ vs. buffer group) (Fig. 4D); however, there was no inhibition of bone metastases by the Ad(E1-).luc treatment. Ad.dcn and Ad(E1-).dcn both produced stronger responses than Ad.luc alone ($p < 0.01$). There were no statistical differences in the rate of tumor growth between Ad.dcn and Ad(E1-).dcn groups (Fig. 4D). On day 22, tumor sizes in Ad(E1-).dcn- and Ad.dcn-treated groups were significantly smaller than the buffer group ($p < 0.01$ Ad(E1-).dcn vs. buffer group, and $p < 0.01$ Ad.dcn vs. buffer group) (Fig. 4E). These results indicated that both Ad.dcn and Ad(E1-).dcn are effective at inhibiting the progression of established breast cancer bone metastases *in vivo*.

Systemic delivery of Ad.dcn reduces tumor burden and inhibits bone destruction

At the terminal time point, tumor burden in the tibia and femur was evaluated by H&E staining, with representative images shown in Fig. 5A. Tumor areas delineated by the yellow line (Fig. 5A) were quantified. Ad.luc, Ad.dcn, and Ad(E1-).dcn all reduced tumor burden significantly ($p < 0.05$ Ad.luc vs. buffer group; $p < 0.01$ Ad(E1-).dcn vs. buffer group; $p < 0.001$ Ad.dcn vs. buffer group) (Fig. 5B).

Because breast cancer bone metastases result in bone destruction, randomly selected bone samples from each group were examined for the osteolytic bone destruction by synchrotron microCT. In the 3D renderings, Ad.dcn-treated groups and the normal bones did not show visible bone destruction; however, all other treatment groups have visible lytic

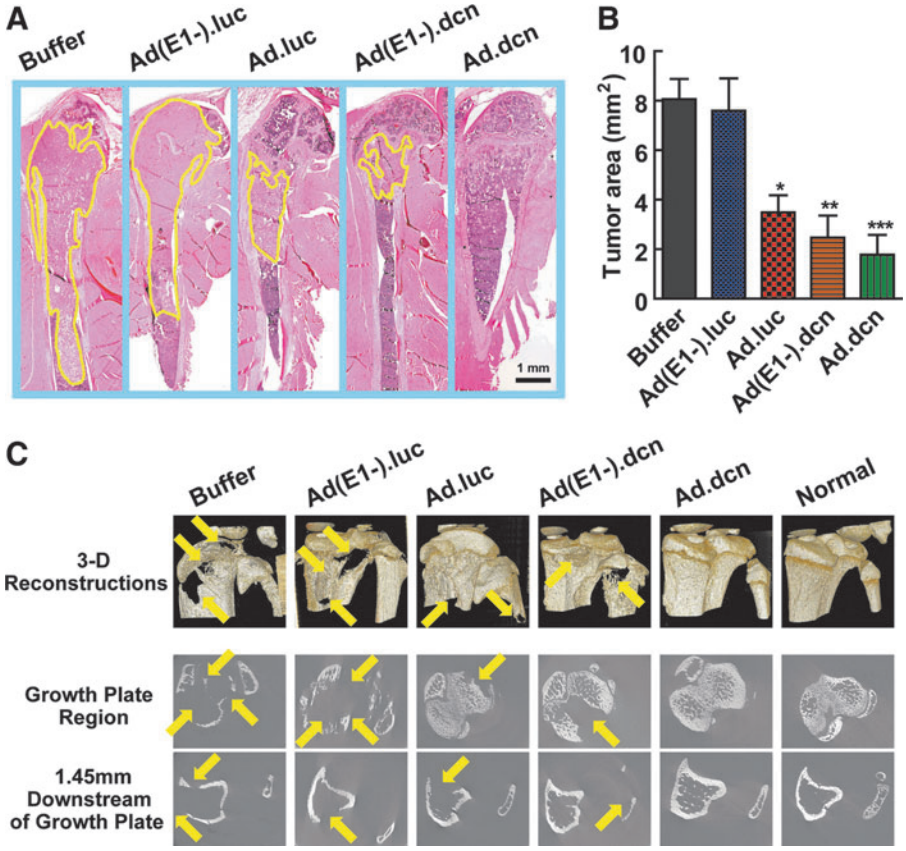

Figure 5. Effects of adenoviral vectors on bone metastasis progression of breast cancer: histomorphometric and micro-computed tomography (microCT) analysis. **(A)** Representative images of longitudinal, midsagittal hematoxylin and eosin (H&E) staining of tibia and femur (obtained on day 22) sections are shown. **(B)** Tumor areas outlined by yellow lines in panel B were used to calculate the tumor burden, and the statistical data are shown. **(C)** Representative 3D renderings of the tibia bones from the buffer-, Ad(E1-).luc-, Ad(E1-).dcn-, Ad.luc-, and Ad.dcn-treated and normal mice (top panel); microCT slices near the growth plate (middle panel) and 1.45 mm distal of the growth plate (lowest panel). Arrows indicate the sites of bone osteolytic destruction/tumor lesions. Data in panel B were derived from 10 mice per group (*$p < 0.05$; **$p < 0.01$; ***$p < 0.001$).

lesions (Fig. 5C, top panel). Extensive trabecular and cortical bone destruction was present in the buffer and Ad(E1-).luc-treated groups, and some bone destruction was also observed in the images from the Ad(E1-).dcn- and Ad.luc-treated groups (Fig. 5C, bottom two panels). Statistical analysis was not possible as too few replicates were imaged, but the data suggested that Ad.dcn could protect the bone architecture and prevent the osteolytic bone destruction induced by the metastatic lesions.

Osteolytic bone destruction was further evaluated by measuring known biomarkers. Bone slices were stained for the TRAP-positive cells. The representative images of the bone–tumor interface are shown in Fig. 6A, with arrows pointing to multinucleated mature osteoclasts. Only the Ad.dcn treatment resulted in a significant reduction in the osteoclast number ($p < 0.01$ vs. buffer group) (Fig. 6B). In this model, hypercalcemia is associated with bone destruction[12]; therefore, serum calcium levels were also examined. Ad.luc, Ad(E1-).dcn, and Ad.dcn treatments inhibited the increase in serum calcium levels ($p < 0.05$ Ad.luc vs. buffer group, $p < 0.01$ Ad(E1-).dcn vs. buffer group and $p < 0.001$ Ad.dcn vs. buffer group) (Fig. 6C). However, there was no significant reduction in the calcium levels in the Ad(E1-).luc-treated group. To confirm the production of decorin, decorin levels in the mice sera were measured at the terminal time point. Results showed that mice administered with Ad.dcn or Ad(E1-).dcn produced decorin; however, there was no detectable serum decorin in the Ad.luc-, Ad(E1-).luc-, or buffer-treated groups (Fig. 6D). Thus, in conclusion, our data indicate that an oncolytic adenovirus engineered to express decorin can suppress a triple-negative breast carcinoma, in nude mice, by inhibiting bone metastases and protecting against osteolytic bone destruction.

DISCUSSION

Bone metastasis is a multistep process in which bone microenvironment provides a fertile soil for the growth of tumor cells. The vicious cycle between the tumor cells and the bone microenvironment

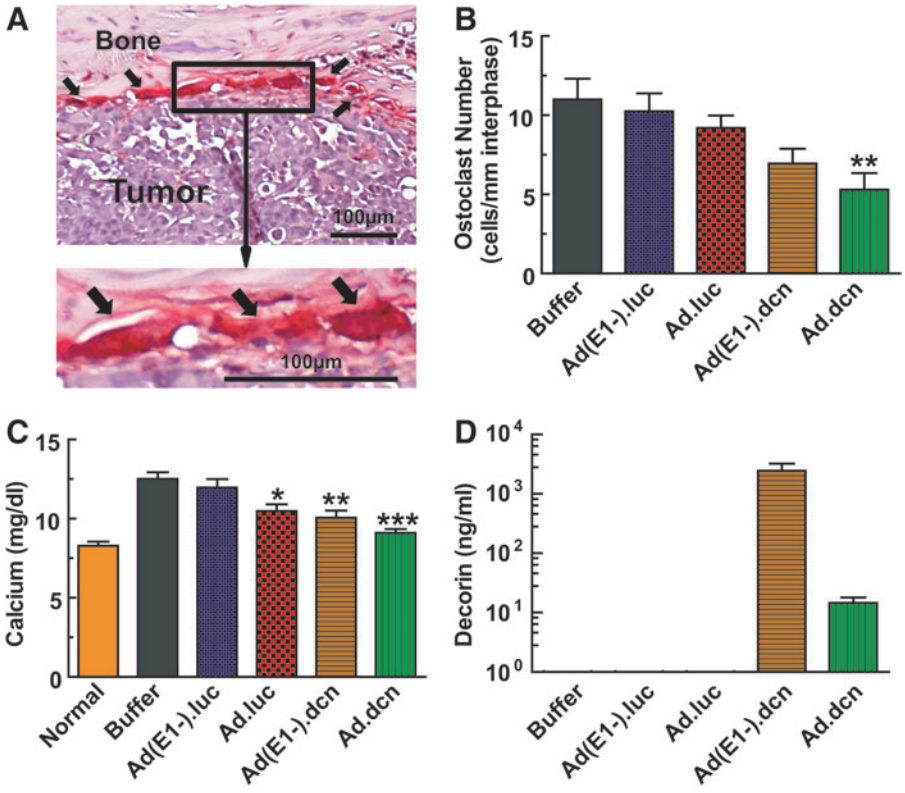

Figure 6. Effects of adenoviral vectors on bone metastasis progression of breast tumor: osteoclast numbers and serum calcium analysis. **(A)** Representative images of TRAP staining of bone sections isolated from various groups on day 22. Arrows indicate multinucleated TRAP-positive osteoclasts, and the scale bar equals 100 μm. **(B)** Osteoclast numbers per millimeter were calculated at the tumor–bone interface in each group ($n = 10$ samples per group). **(C)** Serum calcium concentration on day 22 was measured by a commercial kit; $n = 10$ mice per group. **(D)** Adenoviral-mediated decorin expression in serum was detected by ELISA on day 22. Data in panels B–D were derived from 10 mice per group (*$p < 0.05$; **$p < 0.01$; ***$p < 0.001$).

promotes tumor progression and bone destruction by releasing various cytokines and osteolytic factors.[11,38–40] Therefore, any approach to target bone metastases must ideally target both the tumor cells as well as the tumor–bone microenvironment.

Our results have indicated that both Ad.dcn, a replicating adenovirus, and Ad(E1-).dcn, a nonreplicating adenovirus carrying the decorin gene, inhibit progression of bone metastases, reduce tumor burden, and decrease bone destruction. A nonreplicating virus Ad(E1-).luc did not yield any tumoricidal responses, while Ad.luc, a control replicating adenovirus, inhibited bone metastases, indicating the role of viral replication in the inhibition of bone metastases. However, Ad.dcn and Ad(E1-).dcn, in general, produced better antitumor responses than Ad.luc, and this suggests an important role of decorin in destroying bone metastases within this mouse model.

Our studies have indicated that adenoviral-mediated decorin can potentially inhibit skeletal metastasis and bone destruction using the following mechanisms. It inhibits the tyrosine kinase receptor Met, which is consistent with previous observations that decorin can target multiple tyrosine kinase receptors, including Met, EGFR, IGF-IR, VEGFR2, and PDGFRα/β, all of which are oncogenic and can support tumorigenic growth.[22,41–43] We have also shown here that adenovirus-mediated decorin production inhibits VEGFA expression in MDA-MB-231 cells. Because VEGFA is pro-angiogenic, it suggests that decorin-mediated angiostasis might contribute toward antitumor responses. Decorin plays an important role in the modulation of the angiogenic network via transcriptional induction of angiostatic molecules such as thrombospondin-1 and TIMP3, while downregulating HIF-1α and pro-angiogenic proteases such as matrix metalloproteases MMP-9 and MMP-2.[24,25,44–46] We have also shown that adenoviral-mediated decorin production inhibits β-catenin. Aberrant activation of WNT/β-catenin signaling has been suggested to be a key pathway in promoting tumor cell growth, invasion, and metastasis.[47]

Moreover, adenoviral-mediated decorin production also inhibited the migration of MDA-MB-231 cells. It has been demonstrated that decorin can inhibit the migration of cancer cells via the stability of E-cadherin.[48,49] Decorin has also been shown to inhibit collagen I, a protein that is often overexpressed in the tumor stroma. Moreover, targeting collagen I via decorin could promote adenovirus distribution within the tumors, and hence further improve Ad.dcn potency in inhibiting tumor growth as suggested previously.[34] We have shown that ectopic expression of decorin could induce mitochondrial autophagy in MDA-MB-231 cells. It has been reported that autophagy-deficient tumors, caused by epigenetic mutations or alterations in early stages of oncogenesis, are associated with weaker antitumor immune responses to chemotherapy.[50,51] Induction of autophagy has also been suggested to enhance the cell-mediated and adoptive immune responses and hence promote an antitumor response.[52,53] Therefore, decorin restoration might be a potential mechanism for enhancing the antitumor immune response through mitochondrial autophagy. Therefore, a detailed immune analysis after Ad.dcn treatment must be evaluated in immune-competent bone metastasis models. Adenoviral-mediated decorin production has also been shown to inhibit the expression of TGF-β in tumor cells (Chae-Ok Yun, unpublished data), a central player in promoting the vicious cycle within the tumor–bone microenvironment.[30,33,54–59] Thus, decorin-mediated inhibition of TGF-β could also, in part, account for the strong antitumor responses by Ad.dcn observed here.

It should be noted that decorin protein levels in the blood were relatively higher in Ad(E1-).dcn treatment group compared with the Ad.dcn group (Fig. 6D). Our previous studies have indicated that, after the intravenous delivery of Ad5-based viruses in mice, much of the viruses are taken up by the liver.[16,17] Therefore, we believe that the systemic delivery of Ad.dcn and Ad(E1-).dcn would also result in their hepatic uptake, resulting in vector-mediated decorin production and subsequent release in the blood. The oncolytic virus Ad.dcn-infected cells will be readily destroyed by the host (perhaps because of strong innate/cell-mediated immune responses), resulting in reduced gene expression/decorin production. However, the nonreplicating virus Ad(E1-).dcn-infected cells are expected to be relatively more stable in the liver (perhaps because of weaker immune destruction), and thus Ad(E1-).dcn will produce decorin for a comparatively longer duration. Overall, this will result in higher decorin expression (and subsequent release) in Ad(E1-).dcn versus Ad.dcn groups, and thus increased decorin levels in the blood, particularly at later time points (day 22).

Based on our findings, and several important studies from other laboratories as recently reviewed,[25,40,42,43] we propose the following model of Ad.dcn-mediated treatment of breast cancer bone metastases. Upon systemic delivery of Ad.dcn in mice bearing skeletal metastases, adenoviruses are taken up by the tumor cells where they replicate,

triggering tumor cell lyses and causing some tumor destruction. In addition, the decorin protein produced by the vector will be released into the tumor microenvironment. Unfortunately, the currently available antidecorin antibodies could not be used to examine decorin expression in the skeletal tumors *in vivo*. However, in our previous research using similar oncolytic and nonreplicating viruses expressing soluble TGF-β receptorII fused with human IgG (sTGFβRIIFc) gene, we have shown expression of sTGFβRIIFc in the skeletal tumors.[12] Therefore, we expect that human decorin will be also expressed in the skeletal tumors following Ad.dcn and Ad(E1-).dcn vectors. The decorin protein will downregulate tyrosine kinase receptors, including Met, inhibit WNT/β-catenin signaling, and suppress pro-angiogenic factors such as VEGFA. The inhibition of these decorin target genes is expected to inhibit tumor cell growth, migration of cancer cells, and angiogenesis, culminating in the prevention of tumor growth and metastasis. Decorin will also target TGF-β and will break the vicious cycle between the tumor cells and the tumor–bone microenvironment, resulting in the inhibition of bone metastases and bone destruction. In addition, decorin-induced autophagy and the oncolytic virus-mediated tumor destruction resulting in the release of tumor antigens could also potentially elicit the systemic antitumor immune response. In the future, it would be important to examine these proposed steps *in vivo* including adenoviral-mediated decorin production in skeletal tumors, and decorin-mediated inhibition of target genes within the tumors and the surrounding microenvironment in detail. However, based on our studies described here, we believe that Ad.dcn could be a promising candidate for treating breast cancer bone metastases.

ACKNOWLEDGMENTS

This work was funded in part by the National Institutes of Health Grants R01CA12738 (P.S.) and R01 CA39481 and RO1 CA47282 (R.V.I.), and a CTSA Pilot Award (P.S.) from NorthShore University HealthSystem. We are thankful to an anonymous donor for generous philanthropic support. This research used resources of the Advanced Photon Source, a U.S. Department of Energy (DOE) Office of Science User Facility operated for the DOE Office of Science by Argonne National Laboratory under Contract No. DE-AC02-06CH11357. We are thankful to Janardan Khandekar, Theodore Mazzone, Bruce Brockstein, and Michael Caplan for their continuous support.

AUTHOR DISCLOSURE

No competing financial interests exist for any of the authors.

REFERENCES

1. Fontanella C, Fanotto V, Rihawi K, et al. Skeletal metastases from breast cancer: Pathogenesis of bone tropism and treatment strategy. Clin Exp Metastasis 2015. [Epub ahead of print] DOI: 10.1007/s10585-015-9743-0.
2. Mundy GR. Metastasis to bone: Causes, consequences and therapeutic opportunities. Nat Rev Cancer 2002;2:584–593.
3. Hess KR, Varadhachary GR, Taylor SH, et al. Metastatic patterns in adenocarcinoma. Cancer 2006;106:1624–1633.
4. Pantel K, Alix-Panabieres C, Riethdorf S. Cancer micrometastases. Nat Rev Clin Oncol 2009;6:339–351.
5. Guise TA, Brufsky A, Coleman RE. Understanding and optimizing bone health in breast cancer. Curr Med Res Opin 2010;26 Suppl 3:3–20.
6. Coleman RE. Metastatic bone disease: Clinical features, pathophysiology and treatment strategies. Cancer Treat Rev 2001;27:165–176.
7. Lluch A, Cueva J, Ruiz-Borrego M, et al. Zoledronic acid in the treatment of metastatic breast cancer. Anticancer Drugs 2014;25:1–7.
8. Casas A, Llombart A, Martin M. Denosumab for the treatment of bone metastases in advanced breast cancer. Breast 2013;22:585–592.
9. Candelaria-Quintana D, Dayao ZR, Royce ME. The role of antiresorptive therapies in improving patient care in early and metastatic breast cancer. Breast Cancer Res Treat 2012;132:355–363.
10. Buijs JT, Stayrook KR, Guise TA. TGF-beta in the bone microenvironment: Role in breast cancer metastases. Cancer Microenviron 2011;4:261–281.
11. Akhtari M, Mansuri J, Newman KA, et al. Biology of breast cancer bone metastasis. Cancer Biol Ther 2008;7:3–9.
12. Hu Z, Zhang Z, Guise T, Seth P. Systemic delivery of an oncolytic adenovirus expressing soluble transforming growth factor-beta receptor II-Fc fusion protein can inhibit breast cancer bone metastasis in a mouse model. Hum Gene Ther 2010;21:1623–1629.
13. Hu Z, Gerseny H, Zhang Z, et al. Oncolytic adenovirus expressing soluble TGFbeta receptor II-Fc-mediated inhibition of established bone metastases: A safe and effective systemic therapeutic approach for breast cancer. Mol Ther 2011;19:1609–1618.
14. Zhang Z, Hu Z, Gupta J, et al. Intravenous administration of adenoviruses targeting transforming growth factor beta signaling inhibits established bone metastases in 4T1 mouse mammary tumor model in an immunocompetent syngeneic host. Cancer Gene Ther 2012;19:630–636.
15. Hu Z, Gupta J, Zhang Z, et al. Systemic delivery of oncolytic adenoviruses targeting transforming growth factor-beta inhibits established bone metastasis in a prostate cancer mouse model. Hum Gene Ther 2012;23:871–882.
16. Zhang Z, Krimmel J, Hu Z, Seth P. Systemic delivery of a novel liver-detargeted oncolytic adenovirus causes reduced liver toxicity but maintains the antitumor response in a breast cancer bone metastasis model. Hum Gene Ther 2011;22:1137–1142.
17. Xu W, Zhang Z, Yang Y, et al. Ad5/48 hexon oncolytic virus expressing sTGFbetaRIIFc produces reduced hepatic and systemic toxicities and in-

hibits prostate cancer bone metastases. Mol Ther 2014;22:1504–1517.

18. Xu W, Neill T, Yang Y, et al. The systemic delivery of an oncolytic adenovirus expressing decorin inhibits bone metastasis in a mouse model of human prostate cancer. Gene Ther 2015;22:31–40.
19. Iozzo RV, Schaefer L. Proteoglycan form and function: A comprehensive nomenclature of proteoglycans. Matrix Biol 2015;42:11–55.
20. Yamaguchi Y, Mann DM, Ruoslahti E. Negative regulation of transforming growth factor-beta by the proteoglycan decorin. Nature 1990;346:281–284.
21. Zhang C, Tan CK, McFarlane C, et al. Myostatin-null mice exhibit delayed skin wound healing through the blockade of transforming growth factor-beta signaling by decorin. Am J Physiol Cell Physiol 2012;302:C1213–C1225.
22. Neill T, Painter H, Buraschi S, et al. Decorin antagonizes the angiogenic network: Concurrent inhibition of Met, hypoxia inducible factor 1alpha, vascular endothelial growth factor A, and induction of thrombospondin-1 and TIMP3. J Biol Chem 2012;287:5492–5506.
23. Buraschi S, Pal N, Tyler-Rubinstein N, et al. Decorin antagonizes Met receptor activity and down-regulates {beta}-catenin and Myc levels. J Biol Chem 2010;285:42075–42085.
24. Neill T, Jones HR, Crane-Smith Z, et al. Decorin induces rapid secretion of thrombospondin-1 in basal breast carcinoma cells via inhibition of Ras homolog gene family, member A/Rho-associated coiled-coil containing protein kinase 1. FEBS J 2013;280:2353–2368.
25. Neill T, Schaefer L, Iozzo RV. Decorin: A guardian from the matrix. Am J Pathol 2012;181:380–387.
26. Goyal A, Neill T, Owens RT, et al. Decorin activates AMPK, an energy sensor kinase, to induce autophagy in endothelial cells. Matrix Biol 2014;34:46–54.
27. Neill T, Schaefer L, Iozzo RV. Instructive roles of extracellular matrix on autophagy. Am J Pathol 2014;184:2146–2153.
28. Neill T, Torres A, Buraschi S, et al. Decorin induces mitophagy in breast carcinoma cells via peroxisome proliferator-activated receptor gamma coactivator-1alpha (PGC-1alpha) and mitostatin. J Biol Chem 2014;289:4952–4968.
29. Mefford D, Mefford J. Stromal genes add prognostic information to proliferation and histoclinical markers: A basis for the next generation of breast cancer gene signatures. PloS One 2012; 7:e37646.
30. Oda G, Sato T, Ishikawa T, et al. Significance of stromal decorin expression during the progression of breast cancer. Oncol Rep 2012;28:2003–2008.
31. Duncan MB. Extracellular matrix transcriptome dynamics in hepatocellular carcinoma. Matrix Biol 2013;32:393–398.
32. Buraschi S, Neill T, Owens RT, et al. Decorin protein core affects the global gene expression profile of the tumor microenvironment in a triple-negative orthotopic breast carcinoma xenograft model. PloS One 2012;7:e45559.
33. Reed CC, Waterhouse A, Kirby S, et al. Decorin prevents metastatic spreading of breast cancer. Oncogene 2005;24:1104–1110.
34. Choi IK, Lee YS, Yoo JY, et al. Effect of decorin on overcoming the extracellular matrix barrier for oncolytic virotherapy. Gene Ther 2010;17:190–201.
35. Katayose D, Gudas J, Nguyen H, et al. Cytotoxic effects of adenovirus-mediated wild-type p53 protein expression in normal and tumor mammary epithelial cells. Clin Cancer Res 1995;1:889–897.
36. Goldoni S, Humphries A, Nystrom A, et al. Decorin is a novel antagonistic ligand of the Met receptor. J Cell Biol 2009;185:743–754.
37. Dagda RK, Cherra SJ 3rd, Kulich SM, et al. Loss of PINK1 function promotes mitophagy through effects on oxidative stress and mitochondrial fission. J Biol Chem 2009;284:13843–13855.
38. Korpal M, Yan J, Lu X, et al. Imaging transforming growth factor-beta signaling dynamics and therapeutic response in breast cancer bone metastasis. Nat Med 2009;15:960–966.
39. Kang Y, Siegel PM, Shu W, et al. A multigenic program mediating breast cancer metastasis to bone. Cancer Cell 2003;3:537–549.
40. Waning DL, Guise TA. Molecular mechanisms of bone metastasis and associated muscle weakness. Clin Cancer Res 2014;20:3071–3077.
41. Horvath Z, Kovalszky I, Fullar A, et al. Decorin deficiency promotes hepatic carcinogenesis. Matrix Biol 2014;35:194–205.
42. Neill T, Schaefer L, Iozzo R. Oncosuppressive functions of decorin. Mol Cell Oncol 2015;2:e975645.
43. Sofeu Feugaing DD, Gotte M, Viola M. More than matrix: The multifaceted role of decorin in cancer. Eur J Cell Biol 2013;92:1–11.
44. Iozzo RV, Sanderson RD. Proteoglycans in cancer biology, tumour microenvironment and angiogenesis. J Cell Mol Med 2011;15:1013–1031.
45. Fiedler LR, Eble JA. Decorin regulates endothelial cell-matrix interactions during angiogenesis. Cell Adhesion Migration 2009;3:3–6.
46. Grant DS, Yenisey C, Rose RW, et al. Decorin suppresses tumor cell-mediated angiogenesis. Oncogene 2002;21:4765–4777.
47. Yook JI, Li XY, Ota I, et al. A Wnt-Axin2-GSK3beta cascade regulates Snail1 activity in breast cancer cells. Nat Cell Biol 2006;8:1398–1406.
48. Yu X, Zou Y, Li Q, et al. Decorin-mediated inhibition of cholangiocarcinoma cell growth and migration and promotion of apoptosis are associated with E-cadherin in vitro. Tumour Biol 2014;35:3103–3112.
49. Bi X, Pohl NM, Qian Z, et al. Decorin-mediated inhibition of colorectal cancer growth and migration is associated with E-cadherin in vitro and in mice. Carcinogenesis 2012;33:326–330.
50. Morselli E, Galluzzi L, Kepp O, et al. Anti- and pro-tumor functions of autophagy. Biochim Biophys Acta 2009;1793:1524–1532.
51. White E. Deconvoluting the context-dependent role for autophagy in cancer. Nat Rev Cancer 2012;12:401–410.
52. Valdor R, Macian F. Autophagy and the regulation of the immune response. Pharmacol Res 2012;66: 475–483.
53. Ma Y, Galluzzi L, Zitvogel L, Kroemer G. Autophagy and cellular immune responses. Immunity 2013;39:211–227.
54. Gupta J, Robbins J, Jilling T, Seth P. TGFbeta-dependent induction of interleukin-11 and interleukin-8 involves SMAD and p38 MAPK pathways in breast tumor models with varied bone metastases potential. Cancer Biol Ther 2011;11:311–316.
55. Padua D, Massague J. Roles of TGFbeta in metastasis. Cell Res 2009;19:89–102.
56. Tan AR, Alexe G, Reiss M. Transforming growth factor-beta signaling: Emerging stem cell target in metastatic breast cancer? Breast Cancer Res Treat 2009;115:453–495.
57. Onishi T, Hayashi N, Theriault RL, et al. Future directions of bone-targeted therapy for metastatic breast cancer. Nat Rev Clin Oncol 2010;7:641–651.
58. Buijs JT, Stayrook KR, Guise TA. The role of TGF-beta in bone metastasis: Novel therapeutic perspectives. BoneKEy Rep 2012;1:96.
59. Chiechi A, Waning DL, Stayrook KR, et al. Role of TGF-β in breast cancer bone metastases. Adv Biosci Biotechnol 2013;4:15–30.

Received for publication June 24, 2015;
accepted after revision October 2, 2015.

Published online: October 14, 2015.